Novel Analytical Method for Overhang Effects in Surface-Mounted Permanent-Magnet Machines

HAN-KYEOL YEO[ID]1 AND JONG-SUK RO[ID]2
[1]Research and Development Division, Hyundai Motor Company, Hwaseong 18280, South Korea
[2]School of Electrical and Electronics Engineering, Chung-Ang University, Seoul 06974, South Korea

Corresponding author: Jong-Suk Ro (jongsukro@gmail.com)

ABSTRACT The torque and power densities of surface-mounted permanent-magnet (SPM) machines can be improved significantly using an overhang structure. However, it is difficult to analyze and design SPM machines with overhang because a 3D finite-element method (FEM) that uses high computation time is required to consider the overhang effects accurately. To reduce the computation time significantly, we propose an analytical method in which a magnetic equivalent circuit (MEC) model and an analytical solution (AS) of the Laplace and Poisson equations are combined. This method can accurately estimate the performances of SPM machines with overhang as well as significantly reduce the computation time compared with that required for the 3D FEM. The accuracy and generality of the proposed method were verified by comparison with the 3D FEM in different cases.

INDEX TERMS Analytical method, magnetic equivalent circuit (MEC) model, overhang effect, overhang structure, surface-mounted permanent-magnet (SPM) machine.

I. INTRODUCTION

In a radial-flux machine, when the rotor stack length is longer than the stator stack length, as shown in Fig. 1, it is referred to as an overhang. By adopting an overhang structure that provides additional sources and paths of magnetic flux, machine performance parameters such as torque and power densities can be enhanced effectively without expanding the size of the machine [1], [2]. This is so because the space used up by windings is utilized by adopting a rotor overhang structure. Because of these advantages, overhang structures have been used in various types of radial-flux machines such as claw pole machines [3], spoke-type permanent-magnet (PM) machines [4]–[6], surface-mounted PM (SPM) machines [7]–[9], and interior PM (IPM) machines [2].

A 3D finite-element method (FEM) is essential for the accurate assessment of overhang effects, which cause non-uniform magnetic flux distributions in the axial direction. However, the FEM is computationally expensive. Recently, some studies on analysis methods for SPM machines with overhang have been conducted with the goal

The associate editor coordinating the review of this manuscript and approving it for publication was Xiaodong Liang.
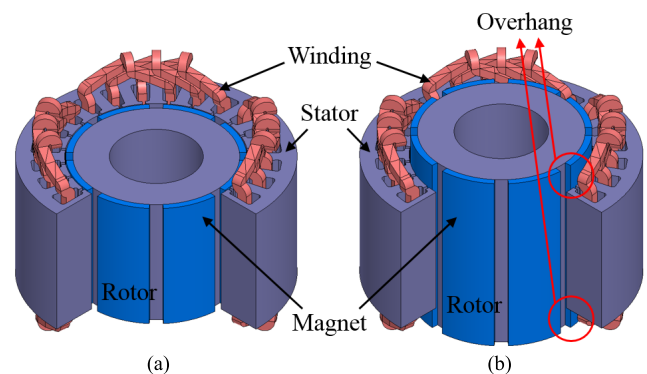
FIGURE 1. SPM machine structures (a) without overhang and (b) with overhang.

of reducing computational time. Firstly, a computational method which was a 2-D FEM combined with the modified permeance coefficient of a PM to consider overhang effects was proposed in [6], [7]. Although this method is simple and effective, a 3D FEM is necessary for calculating the modified coefficient. Moreover, the 2-D FEM is still time-consuming.

Another method is the magnetic equivalent circuit (MEC) model, which involves reluctances and magnetic flux

sources based on the flux paths and material properties of machines. The magnetic flux of an MEC can be calculated easily using Kirchhoff's voltage and current laws. The performance of a machine can be predicted using the calculated air-gap magnetic flux. An MEC with simplified components has been widely used for various types of machines such as transverse flux machines [10], SPM machines [11]–[16], IPM machines [17]–[20], axial-flux PM (AFPM) machines [21], [22], flux-switching PM machines [23], reluctance machines [24], and induction machines [25], [26] with the aim of reducing computational costs significantly. There have also been some attempts to use MECs to consider the overhang effects of SPM machines [27], [28]. In [27], an effective air-gap length between the rotor overhang and stator core was defined for such an MEC. Thus, the average flux densities within the air gap and PM were calculated accurately. However, its applicability was limited to linear SPM machines. In [28], an MEC considering an effective overhang length was proposed. Although the overhang effects of an SPM machine can simply be predicted by the MEC, the accuracy of the MEC might be low in cases where the effective overhang length cannot be appropriately defined. Moreover, the minute magnetic flux distributions are rarely calculated by the MEC because it is composed of simplified components. Therefore, accurate and more generally applicable analysis methods are still required for the analysis and design of SPM machines with overhang.

To calculate minute magnetic flux distributions and predict machine performances accurately, an analytical solution of the Laplace and Poisson equations (AS) has been popularly utilized for various machines such as flux switching machines [29], transverse flux machines [30], SPM machines [31]–[37], IPM machines [38], AFPM machines [39], [40], reluctance machines [41], [42], induction machines [43]. As shown in the aforementioned studies, an AS can be applied to practical machines with complex configurations. However, there have been few studies using an AS because it is difficult to directly calculate complex magnetic flux distributions resulting from overhang through it.

To overcome the aforementioned limitations of using an MEC or an AS when considering overhang effects, we proposed an analytical method (AM) which combined as the two methods. The proposed AM can calculate the minute magnetic flux distributions of an SPM machine with overhang precisely as well as reduce computational costs significantly. To verify the accuracy and wide applicability of the proposed AM, the results were compared with the 3D FEM results for various cases.

II. ANALYTICAL METHOD FOR SPM MACHINE WITH OVERHANG STRUCTURE
We proposed an analytical method (AM) effectively considering the overhang effects of SPM machines. The proposed AM combines an analytical solution of the Laplace and Poisson equations (AS) and a magnetic equivalent

circuit (MEC) model. Utilizing both the AS and the MEC model, the proposed AM can accurately calculate the magnetic flux distributions of SPM machines with overhang as well as effectively reduce computational costs.

To simplify the proposed AM, it is assumed that PMs are radially magnetized and there is no magnetic saturation in the rotor and stator cores. The procedure to assess the performance of SPM machines with overhang consists three steps: 1) estimating the performance of SPM machines without overhang using the AS, 2) calculating the performance enhancement effected by adopting an overhang structure using the MEC, 3) predicting the performances of SPM machines with overhang by combining the results of the AS and MEC. The overhang effects of SPM machines can be estimated accurately and efficiently using this procedure.

A. ANALYTICAL SOLUTION FOR SPM MACHINE WITHOUT OVERHANG STRUCTURE
The back EMF is an essential quantity when predicting machine performance levels. Because the back EMF can be directly calculated from the air-gap magnetic flux density distribution, it is essential to evaluate the air-gap magnetic flux density distribution accurately.

The air-gap magnetic flux density distribution of a slotless SPM machine without overhang in the case of radial magnetization can be precisely calculated via the AS presented in an earlier study [29] as follows:

$$
\begin{aligned}
B_g &= \sum_{n=1,3,5,\ldots}^{\infty} \frac{B_r}{\mu_r} \frac{4}{n\pi} \sin\left(\frac{n\pi\alpha_p}{2}\right) \frac{np\cos(np\theta)}{(np)^2-1} \\
&\times \left[\left(\frac{r}{R_s}\right)^{np-1} \left(\frac{R_m}{R_s}\right)^{np+1} + \left(\frac{R_m}{r}\right)^{np+1} \right] \\
&\times \left[\frac{np-1+2\left(\frac{R_r}{R_m}\right)^{np+1} - (np+1)\left(\frac{R_r}{R_m}\right)^{2np}}{\frac{\mu_r+1}{\mu_r}\left(1-\left(\frac{R_r}{R_s}\right)^{2np}\right) - \frac{\mu_r-1}{\mu_r}\left(\left(\frac{R_m}{R_s}\right)^{2np} - \left(\frac{R_r}{R_m}\right)^{2np}\right)} \right],
\end{aligned}
\tag{1}
$$

where B_r is the magnet remanence, μ_r is the relative recoil permeability of the magnet, α_p is the pole-arc-to-pole-pitch ratio, r is the radius in the middle of the air gap, and p is the number of pole pairs. R_m, R_r, and R_s are the radii of the magnet's outer surface, rotor's outer surface, and stator's inner surface, respectively.

Although most practical SPM machines have a slotted stator structure, slot effects cannot be considered using (1). In this study, the relative air-gap permeance that was calculated from the conformal mapping (CM) of the slot geometry as presented in [32] was combined with (1) to estimate the slot effects of SPM machines accurately. In other words, the air-gap flux density and back EMF in a slotted SPM machine without overhang were calculated accurately by using both the AS and CM, as shown in Fig. 2.
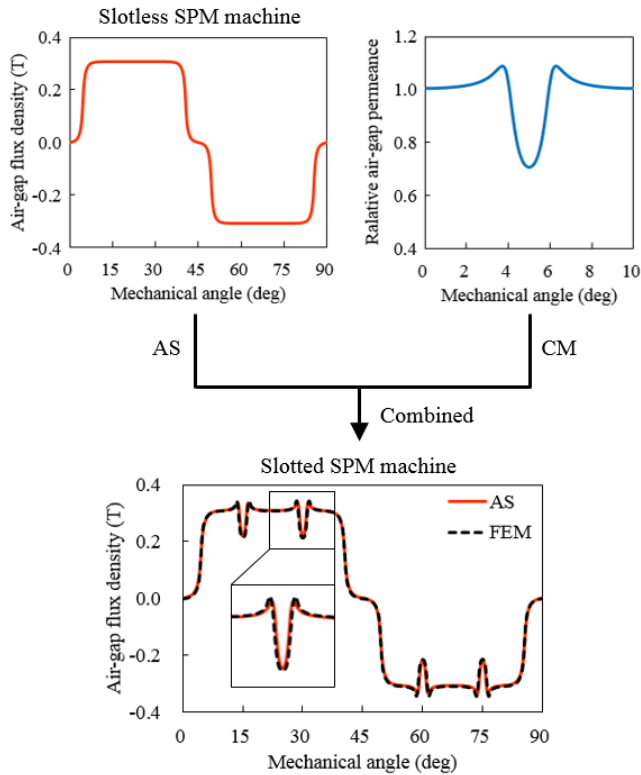
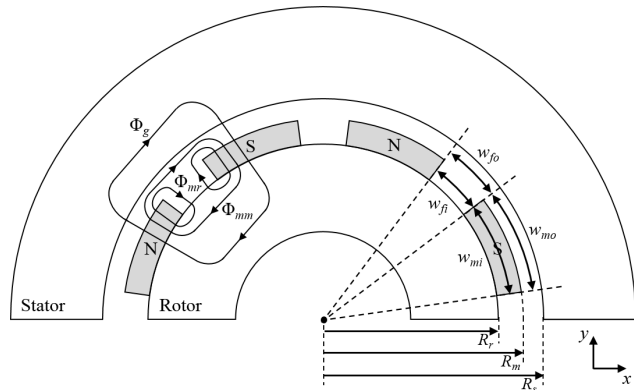FIGURE 2. Procedure of air-gap flux density distribution calculation for slotted SPM machine using AS and CM.

FIGURE 3. SPM machine configuration.

B. MEC FOR SPM MACHINE WITH OVERHANG STRUCTURE

In this section, we propose a simple and effective MEC for calculating the air-gap flux density and back EMF of SPM machines with overhang structures. Some assumptions are made for the simplicity of the proposed MEC: 1) PMs are radially magnetized, 2) no magnetic saturation occurs in the rotor and stator cores, 3) the stator core is slotless.

The main flux path and two leakage flux paths of an SPM machine are shown on the left side of Fig. 3. Φ_g is the main flux flowing from the rotor core to the stator core through the air gap. One of the leakage fluxes is the
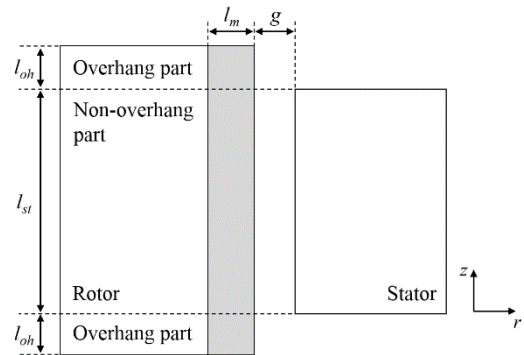

FIGURE 4. Cross-section of SPM machine with overhang structure.

FIGURE 5. MEC for non-overhang part of SPM machine with overhang. (a) Overall MEC. (b) Simplified MEC of (a). (c) Simplified MEC of (b).

magnet-to-magnet leakage flux Φ_{mm}, which travels between two adjacent magnets. The other leakage flux is the magnet-to-rotor leakage flux Φ_{mr}, which travels from the magnet to the rotor core.

An SPM machine with overhang is divided into non-overhang and overhang parts as shown in Fig. 4.

(a)

(b)

(c)

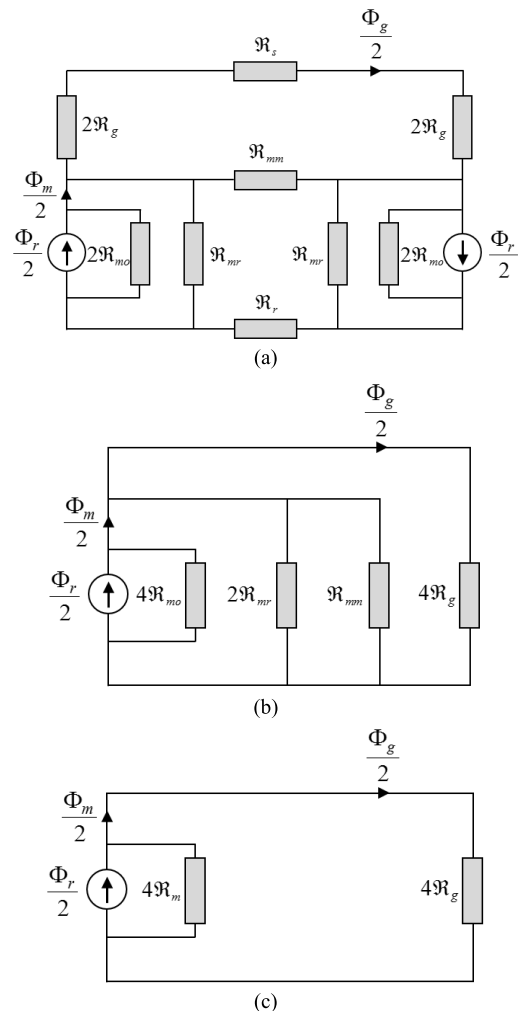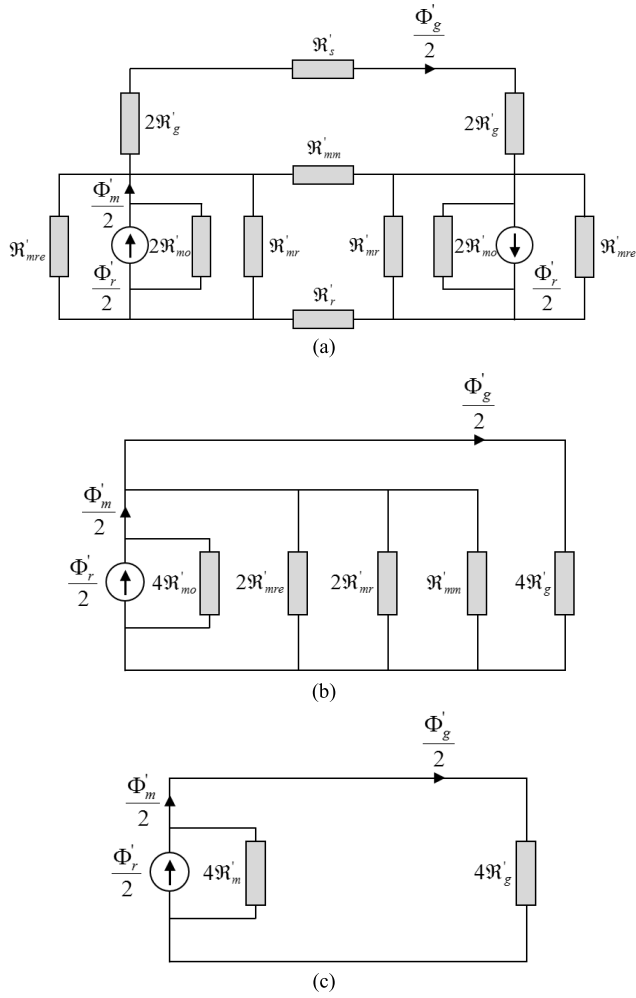**FIGURE 6.** MEC for overhang part of SPM machine with overhang. (a) Overall MEC. (b) Simplified MEC of (a). (c) Simplified MEC of (b).
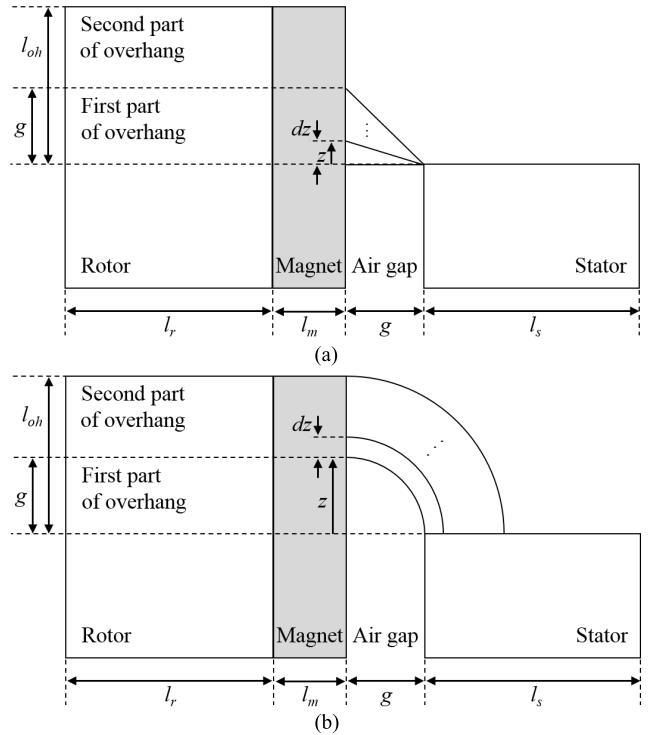

(a)

(b)

FIGURE 7. Modeling of the magnetic flux in the air gap between the overhang and stator core. (a) Straight line permeance model for the first part of overhang. (b) Circular arc permeance model for the second part of the overhang.

The air-gap flux density of the non-overhang part can be calculated accurately using an MEC and considering the aforementioned flux paths. The proposed MEC for the non-overhang part is shown in Fig. 5(a); it is based on [11]. Φ_r is the flux source of one magnet pole and Φ_m is the flux leaving the magnet. $\Re_g$ is the reluctance of the air gap, and $\Re_{mo}$ is the reluctance of the magnet. $\Re_{mm}$ and $\Re_{mr}$ are the reluctances corresponding to Φ_{mm} and Φ_{mr}, respectively. $\Re_r$ and $\Re_s$ are the reluctances of the rotor and stator cores, which are neglected owing to the assumption that no magnetic saturation occurs in the cores. These reluctances are calculated as follows:

$$\Re_g = \frac{g}{\mu_0 \left(w_{mo} + 2g\right) l_{st}} \tag{2}$$

$$\Re_{mo} = \frac{l_m}{\mu_0 \mu_r w_{mi} l_{st}} \tag{3}$$

$$\Re_{mm} = \frac{\pi}{\mu_0 l_{st} \ln\left(1 + \pi g / w_{fo}\right)} \tag{4}$$

$$\Re_{mr} = \frac{\pi}{\mu_0 l_{st} \ln\left(1 + \pi \min\left(g, \frac{w_{fi}}{2}\right) / l_m\right)}, \tag{5}$$

where

$$w_{mi} = \left(\frac{R_r + R_m}{2}\right) \frac{\pi \alpha_p}{p} \tag{6}$$

$$w_{fi} = \left(\frac{R_r + R_m}{2}\right) \frac{\pi \left(1 - \alpha_p\right)}{p} \tag{7}$$

$$w_{mo} = \left(\frac{R_s + R_m}{2}\right) \frac{\pi \alpha_p}{p} \tag{8}$$

$$w_{fo} = \left(\frac{R_s + R_m}{2}\right) \frac{\pi \left(1 - \alpha_p\right)}{p}. \tag{9}$$

In these equations, l_{st} is the stack length, l_m is the magnet thickness, μ_0 is the permeability of the vacuum, and g is the air-gap length. w_{mi} and w_{fi} are the pole-arc width and the width between two adjacent magnets in the middle of the magnet, respectively, and w_{mo} and w_{fo} are the pole-arc width and the width between two adjacent magnets in the middle of the air gap, respectively.

Because the MEC shown in Fig. 5(a) is symmetric, it can be simplified as shown in Fig. 5(b) and (c). Therefore, the air-gap flux can be determined by means of flux division as follows:

$$\Phi_g = \frac{\Re_m \Phi_r}{\Re_m + 4\Re_g} \tag{10}$$

$$\Re_m = = 4\Re_{mo}||2\Re_{mr}||\Re_{mm}. \tag{11}$$

Parameters	Model 1	Model 2	Model 3	Model 4	Model 5
Number of poles/number of slots	8/24	8/24	8/24	8/24	8/9
Radius of rotor's outer surface (R_r), mm	35.5	35.5	35.5	35.5	35.5
Radius of magnet's outer surface (R_m), mm	38.5	38.5	38.5	38.5	38.5
Air-gap length (g), mm	0.5	0.5	0.5	0.5	0.5
Pole-arc-to-pole-pitch ratio (α_p)	0.8	0.8	0.8	0.8	0.8
Magnet remanence (B_r), T	0.4	0.4	0.4	1.07	0.4
Stack length (l_{st}), mm	20	40	60	40	40
Overhang length (l_{oh}), mm	0, 2, 4, 6	0, 4, 8, 12	0, 6, 12, 18	0, 4, 8, 12	0, 4, 8, 12
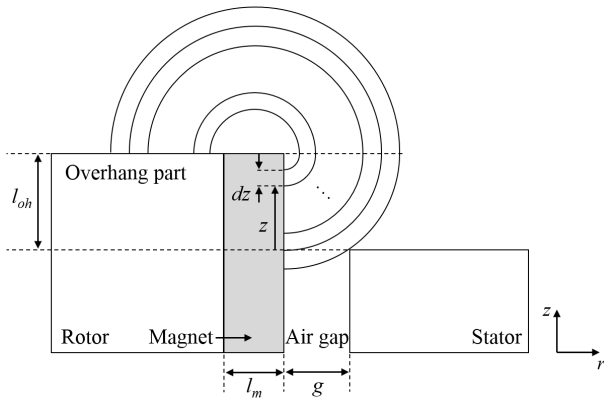
FIGURE 8. Flux path modeling between magnet and rotor end of SPM machine.

Then, the air-gap flux density can be calculated as follows:

$$B_g = \frac{w_{mi} / (w_{mo} + w_{fo})}{(\Re_m + 4\Re_g) / \Re_m} B_r. \tag{12}$$

To consider the overhang effects appropriately, the proposed MEC for the overhang part was as shown in Fig. 6(a).

The air-gap length in the non-overhang part is uniform, whereas the air-gap length in the overhang part varies according to the axial position. In [27], the straight line and circular arc permeance models were proposed to calculate the effective air-gap length between the rotor overhang and stator core as shown in Fig. 7. Therefore, the effective air-gap length was defined as follows:

$$g_e = \begin{cases} \sqrt{g^2 + z^2}, & \text{if } 0 < z \le g \\ \frac{\pi}{2} z, & \text{if } g < z \le l_{oh}, \end{cases} \tag{13}$$

where z is the height in the overhang part. With the effective air-gap length, the reluctances of the overhang part can be obtained as follows:

$$\Re'_g = \frac{g_e}{\mu_0 \left(w_{mo} + 2 \min \left(g_e, \frac{w_{fo}}{2} \right) \right) dz} \tag{14}$$

$$\Re'_{mo} = \frac{l_m}{\mu_0 \mu_r w_{mi} dz} \tag{15}$$

$$\Re'_{mm} = \frac{\pi}{\mu_0 dz \ln \left(1 + \pi \min \left(g_e, \frac{w_{mo}}{2} \right) / w_{fo} \right)} \tag{16}$$

$$\Re'_{mr} = \frac{\pi}{\mu_0 dz \ln \left(1 + \pi \min \left(g_e, \frac{w_{fi}}{2} \right) / l_m \right)}, \tag{17}$$

where dz is the infinitesimal stack length in the overhang part.

The end effects that resulted from the leakage flux from the magnet to the rotor end can be ignored in non-overhang SPM machines. However, the end effects become significant when an overhang structure is adopted. Therefore, the magnet-to-rotor-end leakage flux Φ_{mre} was considered using the flux
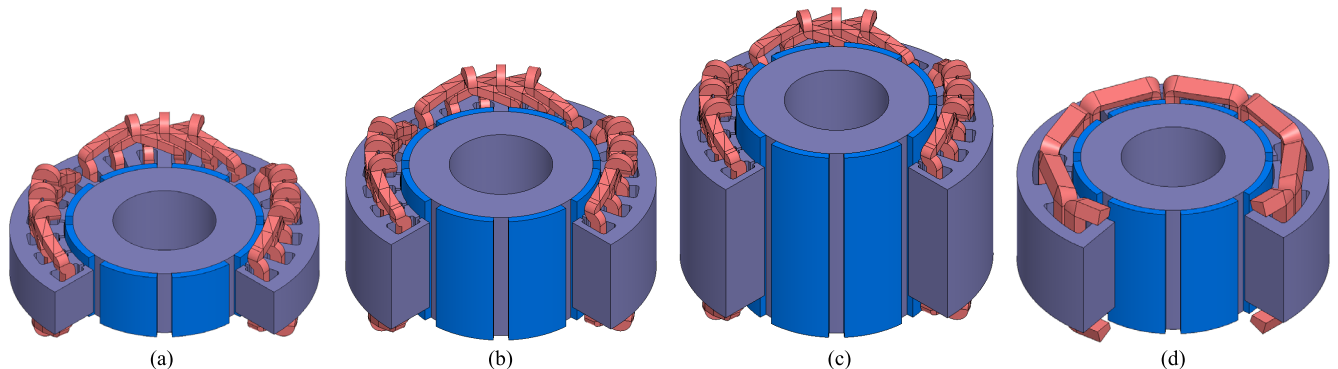
FIGURE 9. Analysis models of SPM machines with overhang structure. (a) Model 1. (b) Models 2 and 4. (c) Model 3. (d) Model 5.

FIGURE 10. Comparison of back EMF in analysis models without overhang. (a) Model 1. (b) Model 2. (c) Model 3. (d) Model 4. (e) Model 5.
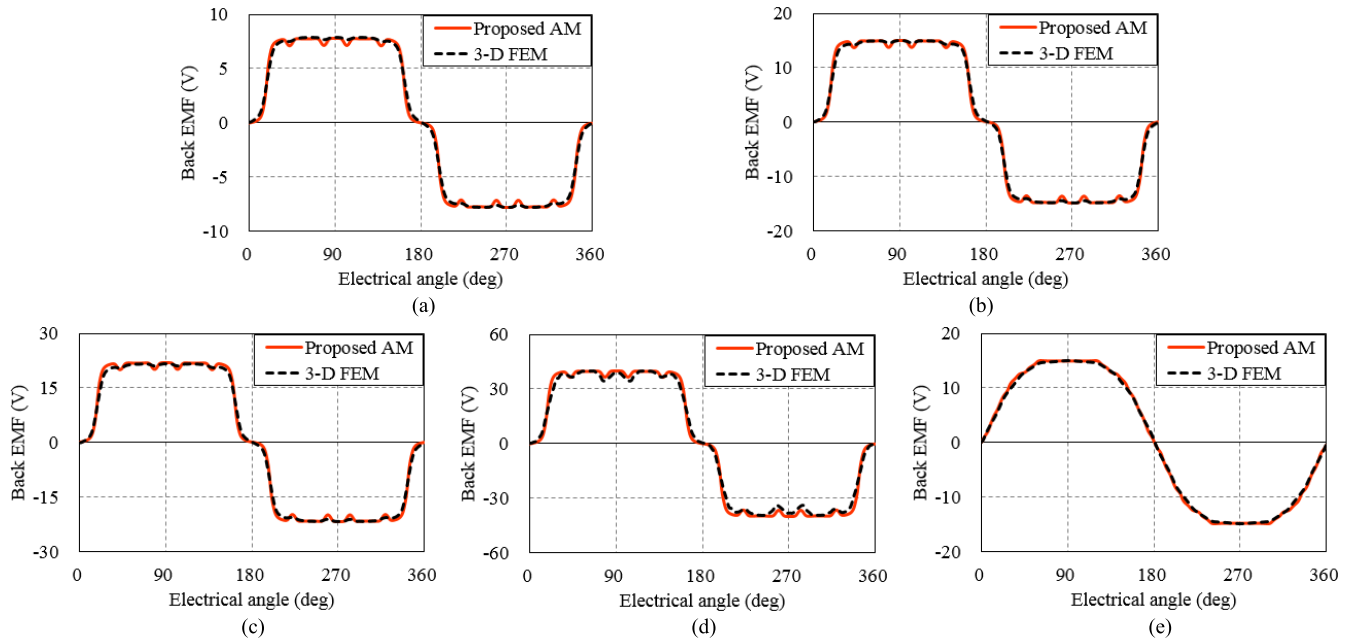
FIGURE 11. Comparison of back EMF in analysis models with overhang when l_{oh} = 20% of l_{st}. (a) Model 1. (b) Model 2. (c) Model 3. (d) Model 4. (e) Model 5.
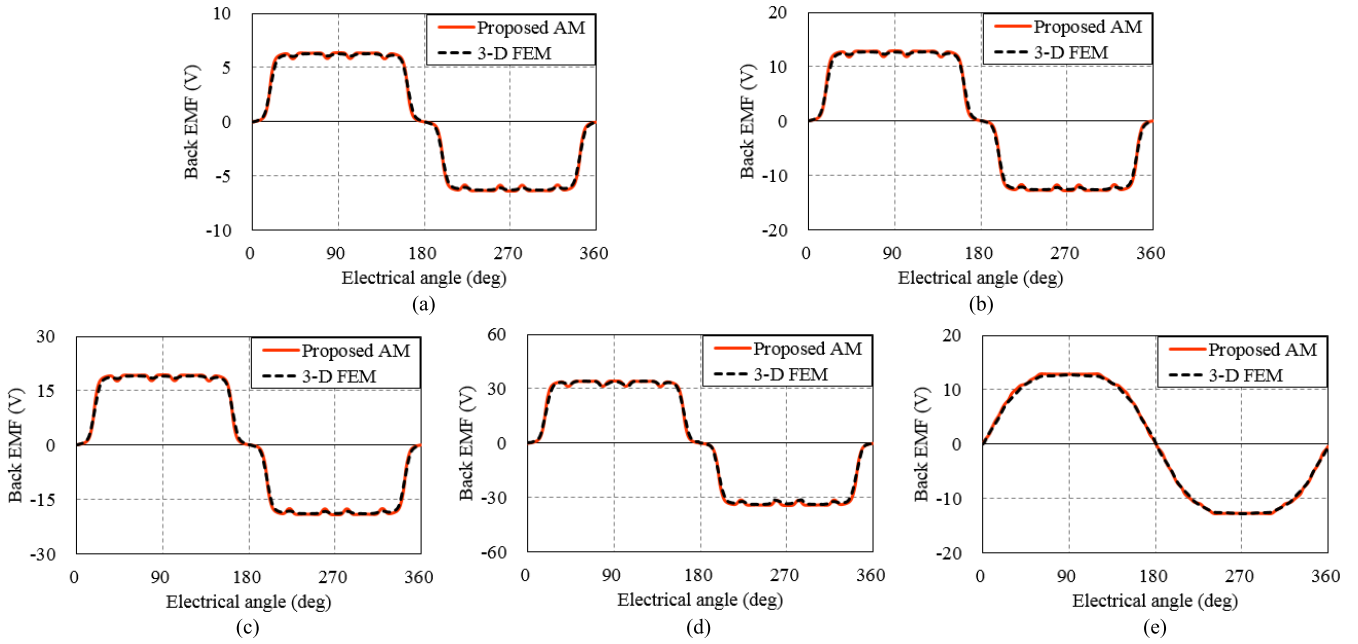
path model shown in Fig. 8. The reluctance corresponding to Φ_{mre} is calculated as follows:

$$\Re'_{mre} = \frac{\frac{\pi}{2}\left(l_m + 3l_{oh} - 3z\right)}{\mu_0 w_{mo} dz}. \tag{18}$$

Owing to its symmetry, Fig. 6(a) can be simplified as Fig. 6(b) and (c). As in the case of the non-overhang part, the air-gap flux of the overhang part can be obtained as follows:

$$\Phi'_g = \frac{\Re'_m \Phi'_r}{\Re'_m + 4\Re'_g} \tag{19}$$

$$\Re'_m = 4\Re'_{mo}||2\Re'_{mr}||\Re'_{mm}||2\Re'_{mre}. \tag{20}$$

Therefore, the air-gap flux density of the overhang part can be calculated as

$$B'_g = \frac{w_{mi}/\left(w_{mo} + w_{fo}\right)}{\left(\Re'_m + 4\Re'_g\right)/\Re'_m} B_r. \tag{21}$$

The overall air-gap flux density of the SPM machine with overhang can easily be obtained by averaging the air-gap flux

TABLE 2. Comparison of peak values of back EMF of SPM machines without and with overhang using proposed AM and 3D FEM.

Analysis model	l_{oh} (mm)	3D FEM (V)	AM (V)	Diff* (%)
Model 1	0	6.3	6.4	-1.3
	2	7.2	7.3	-0.8
	4	7.8	7.8	0.4
	6	8.3	8.2	1.2
Model 2	0	12.7	12.8	-1.4
	4	14.2	14.3	-0.3
	8	14.9	14.9	0.1
	12	15.4	15.4	0.0
Model 3	0	19.0	19.3	-1.4
	6	20.9	21.0	-0.6
	12	21.7	21.8	-0.4
	18	22.0	22.3	-1.3
Model 4	0	33.9	34.4	-1.4
	4	37.9	38.2	-0.6
	8	39.9	40.0	-0.3
	12	41.0	41.2	-0.5
Model 5	0	12.7	12.8	-0.8
	4	14.3	14.3	0.0
	8	14.9	14.9	-0.1
	12	15.2	15.4	-1.1

Diff*: Difference = (3D FEM − AM)/3D FEM × 100.

TABLE 3. Comparison of computation time of back EMF of SPM machines without and with overhang using proposed AM and 3D FEM.

Analysis model	l_{oh} (mm)	3D FEM (V)	AM (V)
Model 1	0	2 h 4 min	
	2	2 h 6 min	
	4	2 h 11 min	10 s
	6	2 h 19 min	
	Total	8 h 40 min	
Model 2	0	4 h 12 min	
	4	4 h 15 min	
	8	4 h 22 min	10 s
	12	4 h 32 min	
	Total	17 h 21 min	
Model 3	0	6 h 27 min	
	6	6 h 31 min	
	12	6 h 43 min	10 s
	18	6 h 58 min	
	Total	26 h 39 min	
Model 4	0	4 h 57 min	
	4	5 h 5 min	
	8	5 h 19 min	10 s
	12	5 h 37 min	
	Total	20 h 58 min	
Model 5	0	18 h 42 min	
	4	18 h 45 min	
	8	18 h 56 min	10 s
	12	19 h 20 min	
	Total	75 h 43 min	

Computer used: Intel Core i7-7700K CPU@4.2 GHz, 32 GB RAM.
h − hour, min − minute, s − second.

densities in the non-overhang and overhang parts. This average value is applied to the air-gap flux density distribution calculated using the AS, as presented in section II-A. In other words, the values of the air-gap flux density distribution are scaled to have the average value estimated by the MEC, as presented in this section. Finally, the scaled air-gap flux density distribution represents that of the SPM machines with overhang.

III. RESULTS AND VERIFICATION

We compared the values of the back EMF obtained using the proposed AM and 3D FEM using five analysis models to verify the validity of the proposed AM. The detailed parameters of the analysis models are listed in Table 1. Fig. 9 shows the analysis models with overhang in which the length of the overhang is equal to 20% of the stack length. Models 1, 2, and 3 are 8-pole/24-slot SPM machines with ferrite magnets of three different stack lengths. Model 4 has the same machine structure as model 2, as shown in Fig. 9(b), but employs a rare-earth magnet. The magnet remanences of the ferrite and rare-earth magnets are 0.4 and 1.07 T, respectively. Model 5 is an 8-pole/9-slot SPM machine with a ferrite magnet. Models 1, 2, 3, and 4 are integer-slot machines, whereas model 5 is a fractional-slot machine with a different stator structure and winding, as shown in Fig. 9(d). All analysis models adopt overhang structures with four different lengths,

i.e., 0%, 10%, 20%, and 30% of the stack length. An overhang length equal to 0% of the stack length implies a non-overhang SPM machine.

As shown in Fig. 10, the back EMF waveforms obtained by the proposed AM and 3D FEM are well-matched in all analysis models without overhang. Moreover, Fig. 11 shows that the proposed AM can accurately calculate the back EMF waveforms for all analysis models with large overhang structures, i.e., when the overhang length is equal to 20% of the stack length.

The results obtained using all analysis models are provided in Table 2. They reveal that the overhang effects vary according to the stack lengths of the SPM machines. In other words, the overhang structures that are as long as 20% of the stack length for models 1, 2, and 3 enhance the back EMFs by 24%, 18%, and 14%, respectively. Moreover, it is confirmed that the overhang effect in every analysis model does not increase linearly but tend to converge as the overhang length increases. Therefore, it is necessary to consider overhang effects accurately in the early design stage of SPM machines with overhang.

As shown in Table 2, the differences between the results obtained from the proposed AM and the 3D FEM in all cases were less than approximately 1.5%. Therefore, the accuracy and usefulness of the proposed AM were verified after considering that the analysis models employed both small and large overhang structures. Further, each model had a different geometry and PM.

Table 3 shows the computation time required for calculating the back EMF of the SPM machines without and with overhang in the proposed AM and 3D FEM. A desktop computer with a 4.2 GHz Intel CPU and 32 GB of RAM was used for this comparison. As shown in Table 3, the proposed AM can significantly reduce the computation time when considering overhang effects by approximately 99.9% as compared to the 3D FEM. For example, the 3D FEM requires 26 h and 39 min for analyzing model 3 with four different overhang lengths, whereas the proposed AM needs only 10 s. Therefore, it is confirmed that the proposed AM can save computational time for the analysis and design of SPM machines with overhang.

IV. CONCLUSION

Overhang is an effective structure for enhancing the torque and power densities of SPM machines. However, considering the overhang effects of SPM machines efficiently and accurately has been challenging. In this work, an analytical method for considering the overhang effects of SPM machines accurately was proposed. The validity of the proposed method was verified by a 3D FEM for different cases. Therefore, the proposed method can generally be used for the analysis and design of SPM machines with overhang. Further, it can significantly reduce computational time as compared to the 3D FEM.

REFERENCES

[1] Y.-D. Chun, J. Lee, and S. Wakao, "Overhang effect analysis of brushless DC motor by 3-D equivalent magnetic circuit network method," *IEEE Trans. Magn.*, vol. 39, no. 3, pp. 1610–1613, May 2003.

[2] H.-K. Yeo, D.-K. Lim, and H.-K. Jung, "Magnetic equivalent circuit model considering the overhang structure of an interior permanent-magnet machine," *IEEE Trans. Magn.*, vol. 55, no. 6, Jun. 2019, Art. no. 8201404.

[3] D.-S. Jung, S.-B. Lim, K.-C. Kim, J. Ahn, S.-C. Go, Y.-G. Son, and J. Lee, "Optimization for improving static torque characteristic in permanent magnet stepping motor with claw poles," *IEEE Trans. Magn.*, vol. 43, no. 4, pp. 1577–1580, Apr. 2007.

[4] K.-C. Kim and J. Lee, "The dynamic analysis of a spoke-type permanent magnet generator with large overhang," *IEEE Trans. Magn.*, vol. 41, no. 10, pp. 3805–3807, Oct. 2005.

[5] W. Zhao, B.-I. Kwon, and T. A. Lipo, "Development and test of a dual-stator, spoke-type ferrite permanent magnet motor with high torque performance for direct-drive applications," in *Proc. Int. Symp. Power Electron., Elect. Drives, Automat. Motion (SPEEDAM)*, Anacapri, Italy, Jun. 2016, pp. 104–109.

[6] J.-Y. Song, J. H. Lee, Y.-J. Kim, and S.-Y. Jung, "Computational method of effective remanence flux density to consider PM overhang effect for spoke-type PM motor with 2-D analysis using magnetic energy," *IEEE Trans. Magn.*, vol. 52, no. 3, Mar. 2016, Art. no. 8200304.

[7] D.-K. Woo, D.-K. Lim, H.-K. Yeo, J.-S. Ro, and H.-K. Jung, "A 2-D finite-element analysis for a permanent magnet synchronous motor taking an overhang effect into consideration," *IEEE Trans. Magn.*, vol. 49, no. 8, pp. 4894–4899, Aug. 2013.

[8] H.-K. Yeo, H.-J. Park, J.-M. Seo, S.-Y. Jung, J.-S. Ro, and H.-K. Jung, "Electromagnetic and thermal analysis of a surface-mounted permanent-magnet motor with overhang structure," *IEEE Trans. Magn.*, vol. 53, no. 6, Jun. 2017, Art. no. 8203304.

[9] J.-G. Lee, H.-K. Yeo, H.-K. Jung, T.-K. Kim, and J.-S. Ro, "Electromagnetic and thermal analysis and design of a novel-structured surface-mounted permanent magnet motor with high-power-density," *IET Electr. Power Appl.*, vol. 13, no. 4, pp. 472–478, Apr. 2019.

[10] S.-I. Jeong, "Design of linear transverse flux machine for stelzer machine using equivalent magnet circuit and FEM," *J. Elect. Eng. Technol.*, vol. 13, no. 4, pp. 1596–1603, Jul. 2018.

[11] R. Qu and T. A. Lipo, "Analysis and modeling of air-gap and zigzag leakage fluxes in a surface-mounted permanent-magnet machine," *IEEE Trans. Ind. Appl.*, vol. 40, no. 1, pp. 121–127, Jan./Feb. 2004.

[12] M.-F. Hsieh and Y.-C. Hsu, "A generalized magnetic circuit modeling approach for design of surface permanent-magnet machines," *IEEE Trans. Ind. Electron.*, vol. 59, no. 2, pp. 779–792, Feb. 2012.

[13] S. Mohammadi and M. Mirsalim, "Analytical design framework for torque and back-EMF optimization, and inductance calculation in double-rotor radial-flux air-cored permanent-magnet synchronous machines," *IEEE Trans. Magn.*, vol. 50, no. 1, Jan. 2014, Art. no. 8200316.

[14] Y.-L. Feng and C.-N. Zhang, "Analytical calculation for predicting the air gap flux density in surface-mounted permanent magnet synchronous machine," *J. Elect. Eng. Technol.*, vol. 12, no. 2, pp. 769–777, Mar. 2017.

[15] C.-S. Jun, B.-I. Kwon, and O. Kwon, "Tolerance sensitivity analysis and robust optimal design method of a surface-mounted permanent magnet motor by using a hybrid response surface method considering manufacturing tolerances," *Energies*, vol. 11, no. 5, p. 1159, May 2018.

[16] P. Naderi, "Magnetic-equivalent-circuit approach for inter-turn and demagnetisation faults analysis in surface mounted permanent-magnet synchronous machines using pole specific search-coil technique," *IET Electr. Power Appl.*, vol. 12, no. 7, pp. 916–928, Aug. 2018.

[17] C. Mi, M. Filippa, W. Liu, and R. Q. Ma, "Analytical method for predicting the air-gap flux of interior-type permanent-magnet machines," *IEEE Trans. Magn.*, vol. 40, no. 1, pp. 50–58, Jan. 2004.

[18] D.-K. Lim, K.-P. Yi, D.-K. Woo, H.-K. Yeo, J.-S. Ro, C.-G. Lee, and H.-K. Jung, "Analysis and design of a multi-layered and multi-segmented interior permanent magnet motor by using an analytic method," *IEEE Trans. Magn.*, vol. 50, no. 6, Jun. 2014, Art. no. 8201308.

[19] P. Liang, Y. Pei, F. Chai, and K. Zhao, "Analytical calculation of D- and Q-axis inductance for interior permanent magnet motors based on winding function theory," *Energies*, vol. 9, no. 8, p. 580, Jul. 2016.

[20] D.-K. Lim and J.-S. Ro, "Analysis and design of a delta-type interior permanent magnet synchronous generator by using an analytic method," *IEEE Access*, vol. 7, pp. 85139–85145, 2019.

[21] Y. Huang, T. Zhou, J. Dong, H. Lin, H. Yang, and M. Cheng, "Magnetic equivalent circuit modeling of yokeless axial flux permanent magnet machine with segmented armature," *IEEE Trans. Magn.*, vol. 50, no. 11, Nov. 2014, Art. no. 8104204.

[22] A. Daghigh, H. Javadi, and H. Torkaman, "Design optimization of direct-coupled ironless axial flux permanent magnet synchronous wind generator with low cost and high annual energy yield," *IEEE Trans. Magn.*, vol. 52, no. 9, Sep. 2016, Art. no. 7403611.

[23] P. Naderi, S. Sharouni, and M. Moradzadeh, "Analysis of partitioned stator flux-switching permanent magnet machine by magnetic equivalent circuit," *Int. J. Elect. Power Energy Syst.*, vol. 111, pp. 369–381, Oct. 2019.

[24] M. Masoumi, M. A. J. Kondelaji, M. Mirsalim, and J. S. Moghani, "Analytical modelling and experimental verification of E-type reluctance motors," *IET Electr. Power Appl.*, vol. 13, no. 1, pp. 110–118, Jan. 2019.

[25] M. Amrhein and P. T. Krein, "Induction machine modeling approach based on 3-D magnetic equivalent circuit framework," *IEEE Trans. Energy Convers.*, vol. 25, no. 2, pp. 339–347, Jun. 2010.

[26] H. Gorginpour, B. Jandaghi, H. Oraee, and E. Abdi, "Magnetic equivalent circuit modelling of brushless doubly-fed induction generator," *IET Renew. Power Gener.*, vol. 8, no. 3, pp. 334–346, Apr. 2014.

[27] H.-K. Yeo, D.-K. Lim, D.-K. Woo, J.-S. Ro, and H.-K. Jung, "Magnetic equivalent circuit model considering overhang structure of a surface-mounted permanent-magnet motor," *IEEE Trans. Magn.*, vol. 51, no. 3, Mar. 2015, Art. no. 8201004.

[28] J.-M. Seo, I.-S. Jung, H.-K. Jung, and J.-S. Ro, "Analysis of overhang effect for a surface-mounted permanent magnet machine using a lumped magnetic circuit model," *IEEE Trans. Magn.*, vol. 50, no. 5, May 2014, Art. no. 8201207.

[29] Y. Yang, J. Chen, B. Yan, C. Zhu, and X. Wang, "Analytical magnetic field prediction of flux switching machine with segmental rotor," *IET Electr. Power Appl.*, vol. 13, no. 1, pp. 91–100, Jan. 2019.

[30] J. R. Anglada and S. M. Sharkh, "Analytical calculation of the torque produced by transverse flux machines," *IET Electr. Power Appl.*, vol. 11, no. 7, pp. 1298–1305, Aug. 2017.

[31] Z. Q. Zhu, D. Howe, E. Bolte, and B. Ackermann, "Instantaneous magnetic field distribution in brushless permanent magnet DC motors, part I: Open-circuit field," *IEEE Trans. Magn.*, vol. 29, no. 1, pp. 124–135, Jan. 1993.

[32] D. Žarko, D. Ban, and T. A. Lipo, "Analytical calculation of magnetic field distribution in the slotted air gap of a surface permanent-magnet motor using complex relative air-gap permeance," *IEEE Trans. Magn.*, vol. 42, no. 7, pp. 1828–1837, Jul. 2006.

[33] A. Rahideh and T. Korakianitis, "Analytical magnetic field distribution of slotless brushless permanent magnet motors—Part I. Armature reaction field, inductance and rotor eddy current loss calculations," *IET Electr. Power Appl.*, vol. 6, no. 9, pp. 628–638, Nov. 2012.

[34] A. Rahideh and T. Korakianitis, "Analytical magnetic field distribution of slotless brushless PM motors. Part 2: Open-circuit field and torque calculations," *IET Electr. Power Appl.*, vol. 6, no. 9, pp. 639–651, Nov. 2012.

[35] Y. Zhou, H. Li, G. Meng, S. Zhou, and Q. Cao, "Analytical calculation of magnetic field and cogging torque in surface-mounted permanent-magnet machines accounting for any eccentric rotor shape," *IEEE Trans. Ind. Electron.*, vol. 62, no. 6, pp. 3438–3447, Jun. 2015.

[36] H. Moayed-Jahromi, A. Rahideh, and M. Mardaneh, "2-D analytical model for external rotor brushless PM machines," *IEEE Trans. Energy Convers.*, vol. 31, no. 3, pp. 1100–1109, Sep. 2016.

[37] R. Guo, H. Yu, T. Xia, Z. Shi, W. Zhong, and X. Liu, "A simplified subdomain analytical model for the design and analysis of a tubular linear permanent magnet oscillation generator," *IEEE Access*, vol. 6, pp. 42355–42367, Jul. 2018.

[38] F. Ma, H. Yin, L. Wei, L. Wu, and C. Gu, "Analytical calculation of armature reaction field of the interior permanent magnet motor," *Energies*, vol. 11, no. 9, p. 2375, Sep. 2018.

[39] S. T. Boroujeni, A. A. Mohammadi, A. Oraee, and H. Oraee, "Approach for analytical modelling of axial-flux PM machines," *IET Electr. Power Appl.*, vol. 10, no. 6, pp. 441–450, Jul. 2016.

[40] M. Baghayipour, A. Darabi, and A. Dastfan, "Detailed analytical method for predicting the steady-state time variations and entire harmonic contents of principal performance characteristics in a non-slotted axial flux permanent magnet motor, considering a precise iron loss model," *IET Electr. Power Appl.*, vol. 12, no. 3, pp. 308–322, Mar. 2018.

[41] E. S. Obe, "Calculation of inductances and torque of an axially laminated synchronous reluctance motor," *IET Electr. Power Appl.*, vol. 4, no. 9, pp. 783–792, Nov. 2010.

[42] L. Jing, J. Cheng, and T. Ben, "Analytical method for magnetic field and electromagnetic performances in switched reluctance machines," *J. Elect. Eng. Technol.*, vol. 14, no. 4, pp. 1625–1635, Jul. 2019.

[43] Y. Wang, H. He, W. Lu, X. Geng, Y. Xu, and Z. Li, "Calculation and analysis of electromagnetic characteristics of double-fed linear motor," *IEEE Access*, vol. 7, pp. 12291–12296, Jan. 2019.

HAN-KYEOL YEO received the B.S. degree in electronic and electrical engineering from Sungkyunkwan University, Suwon, South Korea, in 2012, and the Ph.D. degree in electrical engineering from Seoul National University, Seoul, South Korea, in 2018, through the Combined Master's and Doctorate Program. He is currently with Advanced Electrification Development Team of Hyundai Motor Company. His research interests include analysis and optimal design of electric machines.

JONG-SUK RO received the B.S. degree in mechanical engineering from Hanyang University, Seoul, South Korea, in 2001, and the Ph.D. degree in electrical engineering from Seoul National University (SNU), Seoul, in 2008.

He conducted research at the R&D Center of Samsung Electronics, as a Senior Engineer, from 2008 to 2012. From 2012 to 2013, he was with the Brain Korea 21 Information Technology of SNU, as a Postdoctoral Fellow. He conducted research at the Electrical Energy Conversion System Research Division of the Korea Electrical Engineering and Science Research Institute, as a Researcher, in 2013. From 2013 to 2016, he was with the Brain Korea 21 Plus, SNU, as a BK Assistant Professor. In 2014, he was with the University of BATH, Bath, U.K. He is currently an Associate Professor with the School of Electrical and Electronics Engineering, Chung-Ang University, Seoul. His research interests include the analysis and optimal design of next-generation electrical machines.

• • •